MIJST
MIST International Journal of Science and Technology

Numerical Analysis of Cavitating Flow on Hydrofoil

Md Nur-E-Mostafa[1*], Eare Md Morshed Alam[2], and Mohammad Monir Uddin[3]

[1,2]Department of Science and Humanities, Military Institute of Science and Technology (MIST), Dhaka, Bangladesh
[3]Department of Mathematics and Physics, North South University (NSU), Dhaka, Bangladesh

emails: *[*1]mostafa@sh.mist.ac.bd; [2]morshed5361@gmail.com; and [3]monir.uddin@northsouth.edu*

ARTICLE INFO

Article History:

Received: 28th March 2022
Revised: 30th May 2022
Accepted: 30th August 2022
Published: 29th December 2022

Keywords:

Cavitation value
Mixure model
RNG k-ε *turbulence model*
Irregular flow

ABSTRACT

Numerical study is presented in this work for turbulent cavitating flow pattern simulation on a hydrofoil, using state equation of cavitation model along with combined turbulence model for mixed fluid based on commercial software FLUENT 6.0. This solver is based on finite volume method. Cavitating study yield irregular behavior with the variation of cavitation values (σ). This study is focused on pressure variation, vapor volume fraction, lift and drag forces on the foil section for various cavitation values at 7° angle of attack. Cavitation initiation begins at the foremost surface and covers towards the end chord with reducing cavitation value. Moreover, the change of vapor region pattern is predicted towards the front of the foil. Finally, transitional flow range is observed for σ values 0.8 to 1.2 with large standard deviation.

1. INTRODUCTION

Cavitation is the specific two-phase flow with the process or a period of changing from vaporization to condensation determined by pressure variation without any producing heat. It may be deduced as the suddenly burst of the liquid owing to excessive pressure. According to ref (Brenne 1955), cavitation can be defined, process of bursting a liquid by reducing pressure at approximately constant liquid temperature. Pressure in the liquid is reduced to its vapour pressure at any point in the flow, then the liquid will be boiled at that point and bubbles of vapour will form (Kothandaraman *et al.* 2007). Since the fluid flows into an area of higher pressure the bubbles of vapour will rapidly condense or collapse. This action yields very high dynamic pressure upon the contiguous material surface and as the action is continual and has a large frequency the solid in that region will be gradually damaged. Turbo machine, pump impellers and airfoil type blade etc. are often occurred cavitation and severely damaged repeatedly. Cavitation causes hydrodynamic problem near the contiguous solid surface like increasing drag force, pressure pulsation and changing kinematics fluid flow.

These obvious problems are strongly related to instantaneous behavior of cavitating flow assembly and causes unsteady fluctuations upon the surface at the cavitation area. Hence, good understanding of the problem, the numerical study of cavitating behavior is important for prediction. Therefore, many numerical studies and investigation were carried out in previous (Kubota *et al* 1992, Kunz *et al*. 2000, Schnerr *et al.* 2001, Stutz *et al.* 2002, and Frobenius *et al. 2003).*

In the past decade several methods were developed for numerical simulation of the physics for cavitating flow pattern. Mixture and VOF model is considered the efficient method for the numerical analysis of cavitating study. Most studies are based on the mixture consideration of homogeneous fluid composed by two phase flow which assumed a single mixture flow of fluid-vapor. Two phase mixture model flow was applied for simulation of the present study and previously done by (Karim *et al* 2010 and Mostafa *et al*. 2016). Roohi *et al.* 2012 studied the cavitating behavior by VOF model. A cavitation model is also used here based on phase change and bubble dynamics equation for calculating of unsteady behavior of cavitating flow. Singhal *et al.* (2002) suggested a comprehensive cavitation model by adding the void ratio with vaporization and condensation source terms in a transport equation to regulate the mass shift between two phases. In this study, full cavitation model is used.

Impact of fine mesh generation and chosen of turbulence model is separately analyzed by comparing numerical values of lift coefficent and drag coefficient for non-cavitating flow previously (Karim *et al.*, 2010; Mostafa *et al*., 2016). To calculate unsteady behavior of cavitation around the hydrofoil, we used RNG k-ε turbulence model with improved wall function. Now, the flow pattern of pressure

distribution, contour of pressure coefficient and vapor volume fraction on the top foil surface is separately analyzed. Peak values of pressure coefficient are found increasing in cavitation zone with the decrease of σ values.

2. NUMERICAL SIMULATION

To capture cavitation zone over the hydrofoil, implicit finite volume scheme allied with multiphase mixture model and bubble dynamic cavitation model are used. We applied RNG k-ε turbulence model including improved wall function to comprehend the boundary layer. Calculation of Reynolds number in this work is 5.9×10^{-5} where foil chord length is considered the characteristics dimension. Amount of y^+ is 5-15 obtained by (Karim *et al.*, 2010). Second order central difference approximation is applied to discretize the pressure, viscosity and source terms. In addition, in the momentum equation, the convective term is discretized by implicit second order approximation. Semi-Implicit Method for Pressure-Linked Equations (SIMPLE) is a pressure based solver which is used to solve the incompressible equation

3. MULTIPHAGE MIXTURE MODEL

To modelled the cavitating flows, a mixture model of multiphase flow is applied. Density (ρ_m) of mixture is linked with vapor mass fraction (f_v). In this study, it is derived from the transport equation and turbulence model equation as well as momentum and mass conservation equations. Density of mixture and mass fraction (f_v) of fluid vapour relation was showed by (Dular *et al.* 2005) as follows.

$$\frac{1}{\rho_m} = \frac{f_v}{\rho_v} + \frac{1-f_v}{\rho_l} \tag{1}$$

The relation between vapour phase volume fraction (α_v) and vapour phase mass fraction (f_v) is obtained as:

$$\alpha_v = f_v \frac{\rho_m}{\rho_v} \tag{2}$$

Mass conservation equation for mixture flow is:

$$\frac{\partial}{\partial t}(\rho_m) + \nabla.(\rho_m \vec{v}_m) = 0 \tag{3}$$

Equation of momentum conservation for the mixture flow is:

$$\frac{\partial}{\partial t}(\rho_m \vec{v}_m) + \nabla.(\rho_m \vec{v}_m \vec{v}_m) = -\nabla p + \nabla.[\mu_m(\nabla \vec{v}_m + \nabla \vec{v}_m^T)] + \rho m \vec{g} + \vec{F} \tag{4}$$

The vapour transport equation is:

$$\frac{\partial}{\partial t}(\rho_m f_v) + \nabla.(\rho_m \vec{v}_m f_v) = M_e - M_c \tag{5}$$

4. CAVITATION MODEL

It is considered that, in cavitating situations, the operating fluid consists of mixture of vapour, non-condensable gas and liquid. The liquid evaporation and vapour condensation expression are defined as M_e and M_c respectively which are added in the vapour transport equation. The comprehensive cavitation model is assumed on focusing the transport equations as:

$$M_e = C_e \frac{\sqrt{k}}{\gamma} \rho_l \rho_v \sqrt{\frac{2}{3}\frac{p_v - p}{\rho_l}} (1 - f_v - f_g) \; when \; p < p_v \tag{6}$$

$$M_c = C_c \frac{\sqrt{k}}{\gamma} \rho_l \rho_l \sqrt{\frac{2}{3}\frac{p_v - p}{\rho_l}} f_v \; when \; p > p_v \tag{7}$$

Where the proposed numerical value of empirical constants C_e is 0.02 and C_c is 0.01. In addition, other notation and symbols represents the usual meaning.

5. RNG $k-\varepsilon$ TURBULENCE MODEL

By analyzing the turbulence model in FLUENT, we picked out the RNG $k-\varepsilon$ model for this study. This model is found effective in precisely resolving the near wall zone when the two phase model is used. Choudhury (1993) derived the RNG $k-\varepsilon$ model from the instantaneous Navier-Stockes equation using mathematical procedure called "renormalization group" (RNG). The analytical derivation is almost alike in feature to the standard $k-\varepsilon$ model but includes an extra terms R_ε in its ε equation. The additional term enhances the precision for quickly stained flows significantly. The state equations of the RNG $k-\varepsilon$ model are known by:

$$\frac{\partial}{\partial t}(\rho k) + \frac{\partial}{\partial x_i}(\rho k u_i) = \frac{\partial}{\partial x_j}\left(\alpha_k \mu_{eff} \frac{\partial k}{\partial x_j}\right) + G_k + G_b - \rho\epsilon - Y_m + S_k \tag{8}$$

$$\frac{\partial}{\partial t}(\rho \varepsilon) + \frac{\partial}{\partial x_i}(\rho \varepsilon u_i) = \frac{\partial}{\partial x_j}\left(\alpha_\varepsilon \mu_{eff} \frac{\partial \varepsilon}{\partial x_j}\right) + C_{1\varepsilon}\frac{\varepsilon}{k}(G_k + C_{3\varepsilon}G_b) - C_{2\varepsilon}\rho\frac{\varepsilon^2}{k} - R_\varepsilon + S_\varepsilon \tag{9}$$

where, $C_{1\varepsilon} = 1.42$ and $C_{2\varepsilon} = 1.68$.

The additional term R_ε included in Equation (14) is given as follows:

$$R_\varepsilon = \frac{C_\mu \rho \eta^3 (\eta - \eta/\eta_0)}{1+\beta\eta^3} \frac{\varepsilon^2}{k} \tag{10}$$

where, $\eta \equiv Sk/\varepsilon, \eta_0 = 4.38, \quad \beta = 0.012$

6. FLOW GEOMETRY AND COMPUTATIONAL AREA

CAV2003 hydrofoil cross section is placed in Figure 1 which demonstrate a diagrammatic view geometry and calculation domain. It is located at attack of angle 7° with nominally two dimensional configuration. The leading surface equation of the axisymmetric foil is shown in equation (11):

$$\bar{y} = 0.11858(\bar{x})^{\frac{1}{2}} - 0.02972(\bar{x}) + 0.00593(\bar{x})^2 + -0.07272(\bar{x})^3 + -0.002207(\bar{x})^4 \tag{11}$$

Where $\bar{x} = x/c$ and $\bar{y} = y/c$ are denoted as dimensionless quantity and c is chord of length 0.1m. The flow field is considered incompressible fluid which moving from left flow field to right flow field along the hydrofoil. The computational flow field domain is chosen of dimension 10c length in the direction of x-axis and height 4c in the direction of y-axis. The hydrofoil is set up at the central of the calculating domain. The proper boundary conditions of all boundaries are also shown in Figure 1. The uniform flow velocity profile is fixed 6 m/s at the entrance boundary

condition. Symmetry boundary type is considered as a slip wall illustrated in Figure 1. The constant pressure boundary outlet condition is presented at the far field of the domain. We apply foil surface as no-slip wall.

In order to select a fine grid lines in mesh for flow domain, a detailed grid analysis was done in past by the published work ref (Karim *et al.* 2010). A particular grid with computational domain is illustrated in Figure 2.

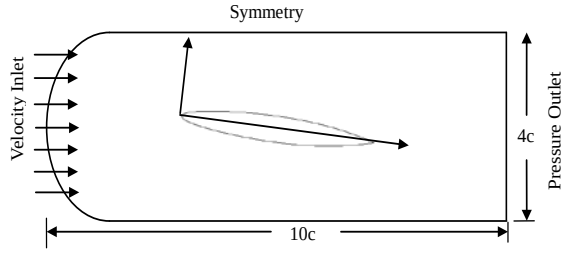

Figure 1: Diagrammatic view of CAV2003 hydrofoil, flow domain and set boundary condition

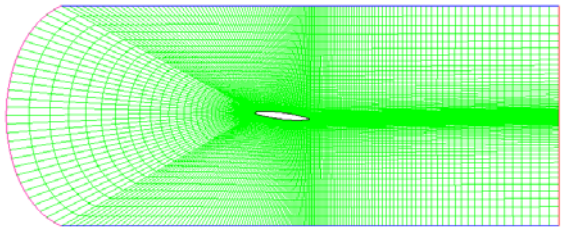

Figure 2: A inclusive view of fine grid lines with computational domain

7. RESULTS AND DISCUSSION

The convergence benchmark is resolved by observing various features of estimation of flow, such as inlet velocity and static pressure at the back of hydrofoil in the flow field. The computational residual value is taken as 10^{-4}. The mass fraction of non-condensable gas is an important parameter of FLUENT. It is observed that results are reasonably sensitive to the value of non-condensable gas. Based on the initial test calculation the convergence criterion value 10^{-6} is found to give rational results and use for the present work. For computation of cavitating flow, the other initial parameters are shown in Table 1.

Table 1
Initial condition for simulation

Parameters	Values
Re	5.9×10^5
Attack angle	7°
Velocity	6.0 m / s
ρ_l	998.0 kg/m^3
ρ_v	0.5542 kg/m^3
μ_l	10^{-3}
P_{ref}	101325 Pa
P_v	98929.32 Pa
Time step	5×10^{-5}
Per time step	30 iteration
μ_v	$1.34 \times 10^{-5} Pa$
Surface tension, γ	0.0717 N/M

For good understanding of the cavitating flow behavior on the hydrofoil, numerical analysis has been done for the various σ values 0.4, 0.8, 0.9, 1.0, 1.1, 1.2, 1.5 and 3.5. We compare the computed result for σ values at 0.8 and 0.4 with published results of different authors for validation purpose and comparative analysis.

The comparison is carried out for the calculating time dependent lift value and drag value with the numerical result of (Pouffary *et al.* 2003; Mortazazadeh *et al.* 2014; Kawamura *et al.* 2003; and Yoshinori *et al.* 2003). As shown in Table 2, the computed time averaged lift values and drag values are seen in well agreement with available result of various researchers. For cavitation number 0.8, the calculated values of lift coefficient and drag coefficient using present method are more consistences and comply with result of (Pouffary *et al.* 2003). Though, there is seen a little inconsistency for the cavitation value 0.4. This phenomenon may be ascribed owing to the fact that many authors used various turbulence models.

The computed pressure variation curve on the suction side of foil top surface at σ values 0.4 & 0.8 is illustrated in Figure 3 and 4 respectively, together with pressure curve of (Kawamura *et al.* 2003). A good consistency trend is observed except in tailing edge. This little discrepancy in magnitude may be happened due to (Kawamura *et al.* 2003) used *k-ω* turbulence model.

Table 2
Lift values and drag values for cavitation numbers at 0.8 & 0.4

	σ value 0.8		*σ value 0.4*	
	lift	**drag**	**lift**	**drag**
Current result	0.442	0.0773	0.214	0.0763
Mortazazadeh	0.413	0.068	-	-
Pouffary	0.4566	0.0783	0.2911	0.0866
Courtier-Delgosha	0.4501	0.0700	0.2001	0.0650
Kawamura	0.3990	0.0470	0.1870	0.0630
Yoshinori	0.4170	0.0638	0.1600	0.0568

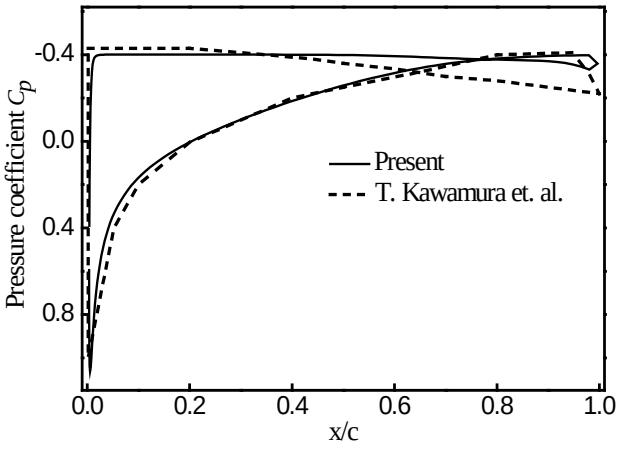

Figure 3: Comparing the variation of pressure coefficient on the top edge of the foil at cavitation values 0.4

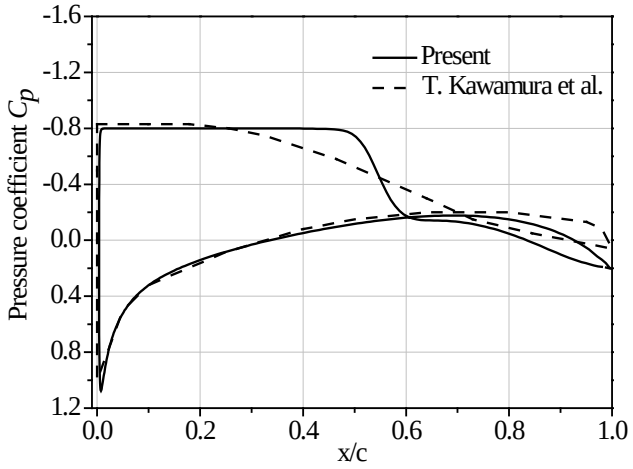

Figure 4: Comparing the variation of pressure coefficient on the top edge of the foil at cavitation values 0.8

The exit pressure distribution on the hydrofoil top surface varied to yield the different cavitation values ($\sigma = 0.4, 0.8, 0.9, 1.0, 1.1, 1.2, 1.5, 3.5$) are presented in Figure 5(a-f). Cavitation initiation starts at the upstream surface of the foil and gradually grows towards the end chord with reducing cavitation value. The maximum values of pressure distribution in area of cavitation is developed with the decreasing of cavitation values.

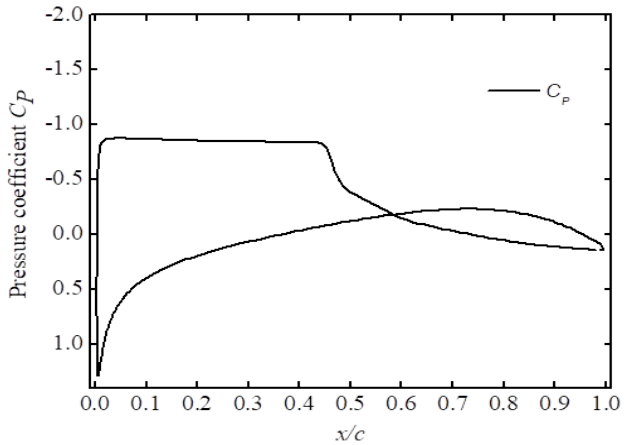

Figure 5 (a): Variation of pressure coefficient on the top edge of the foil at cavitation values 0.9

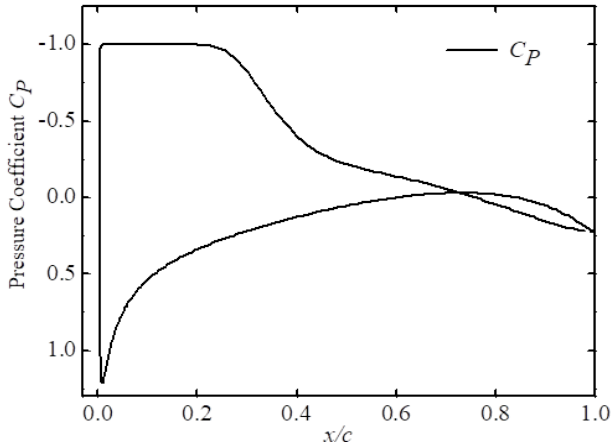

Figure 5 (b): Variation of pressure coefficient on the top edge of the foil at cavitation values 1.0

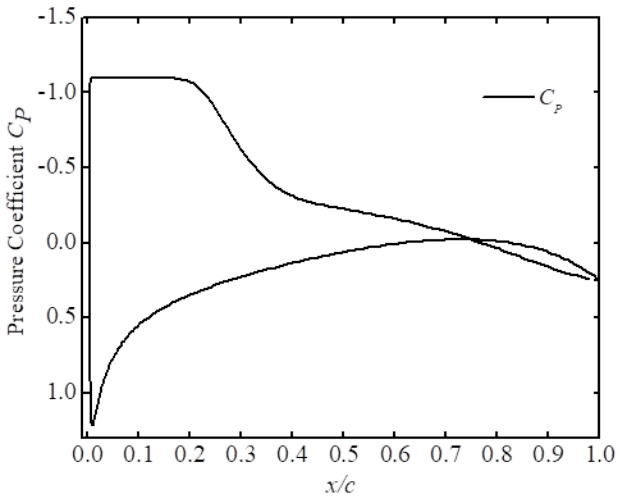

Figure 5 (c): Variation of pressure coefficient on the top edge of the foil at cavitation values 1.1

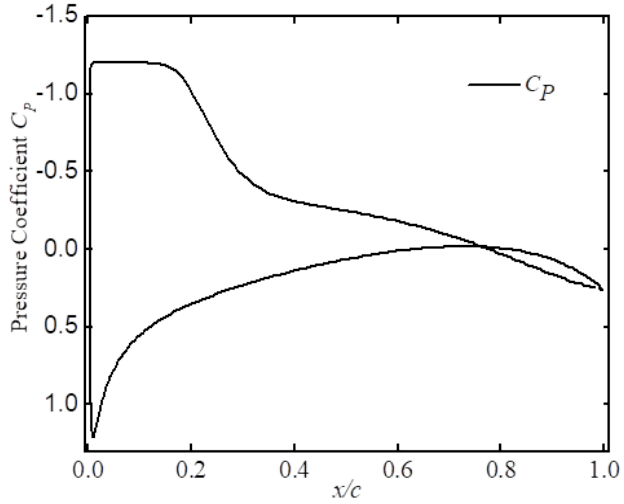

Figure 5 (d): Variation of pressure coefficient on the top edge of the foil at cavitation values 1.2

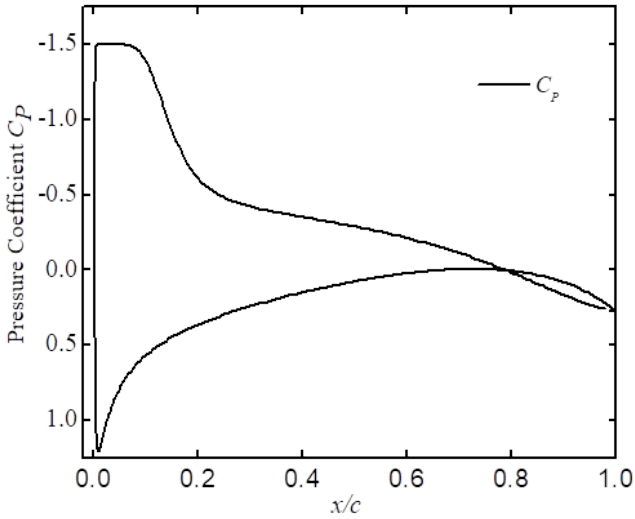

Figure 5 (e): Variation of pressure coefficient on the top edge of the foil at cavitation values 1.5

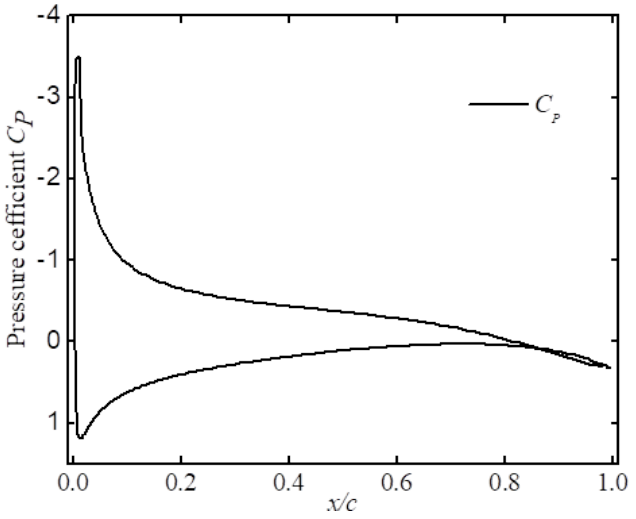

Figure 5 (f): Variation of pressure coefficient on the top edge of the foil at cavitation values 3.5

Lift and drag coefficients time series curves of different σ values 0.8-3.5 are shown in Figure 6 (a-j). It is seen that the time dependent curve is fluctuated around its averaged value because of unsteady nature. The fluctuation gradually decreases with the increasing of cavitation values. The pressure coefficient contours for various cavitation value (0.4-3.5) are shown in Figure 7 (a-f). It is observed that the variation in pressure coefficient relate to the proportion of the volume of voids to volume of solids. These pressure contours show the development of cavity and its magnitude for various cavitation value. The computed result of vapour volume fraction of various σ values appear in Figure 8 (a-f). Very small value of vapour is appeared at σ value 1.5 whereas the full surface is covered with vapour volume at 0.4. As the cavitation values decrease the values of the vapour volume fraction gradually grows to the mid-chord area and vapour region moves to the front of the hydrofoil.

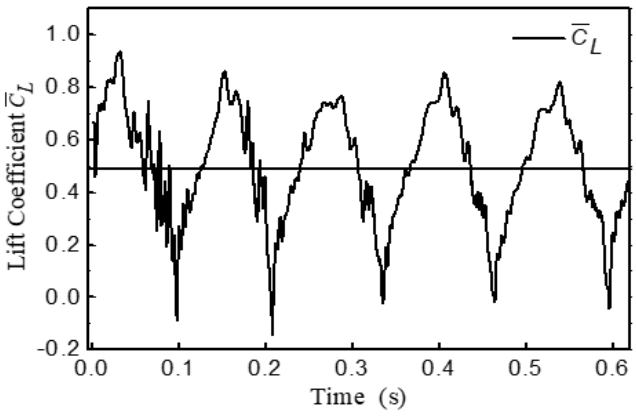

Figure 6(a): Lift coefficient time series for cavitation value 0.8

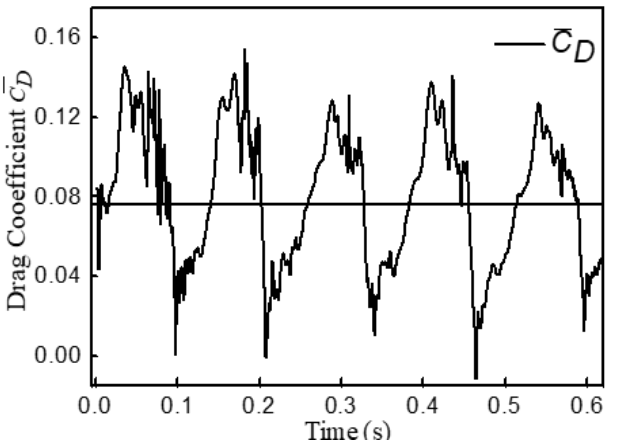

Figure 6(b): Drag coefficient time series for cavitation value 0.8

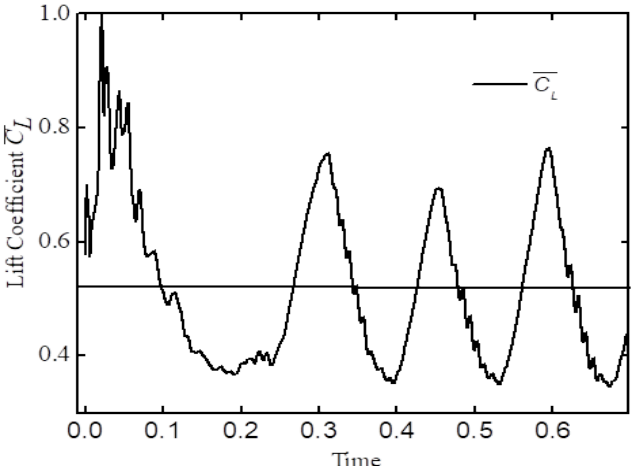

Figure 6(c): Lift coefficient time series for cavitation value 0.9

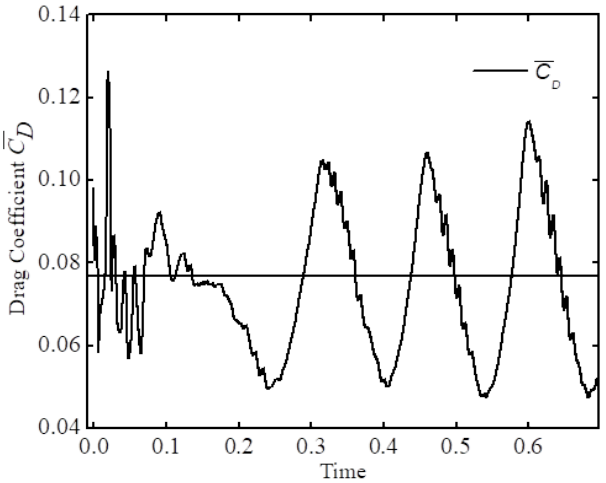

Figure 6(d): Drag coefficient time series for cavitation value 0.9

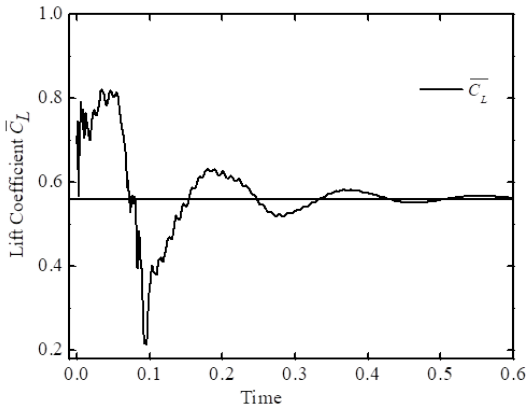

Figure 6(e): Lift coefficient time series for cavitation value 1.0

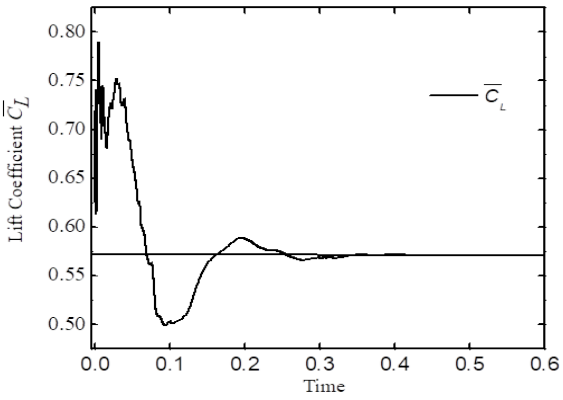

Figure 6(i): Lift coefficient time series for cavitation value 1.5

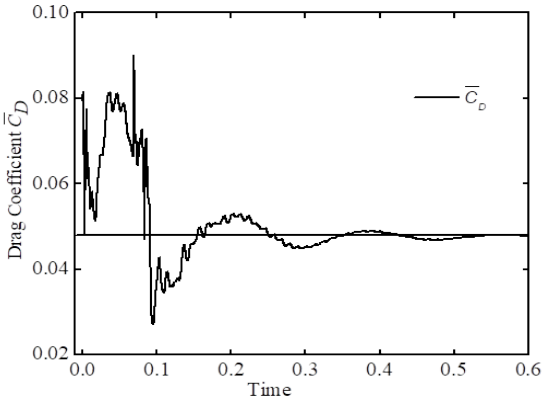

Figure 6(f): Drag coefficient time series for cavitation value 1.0

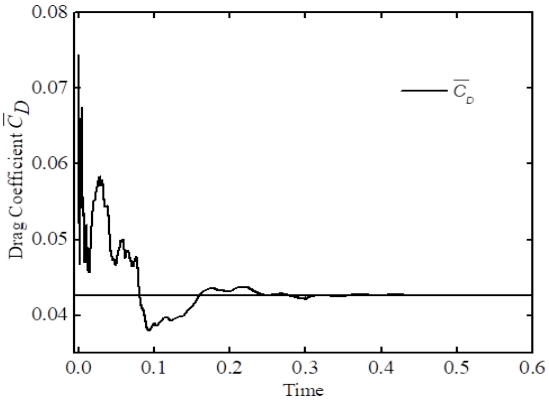

Figure 6(j): Drag coefficient time series for cavitation value 1.5

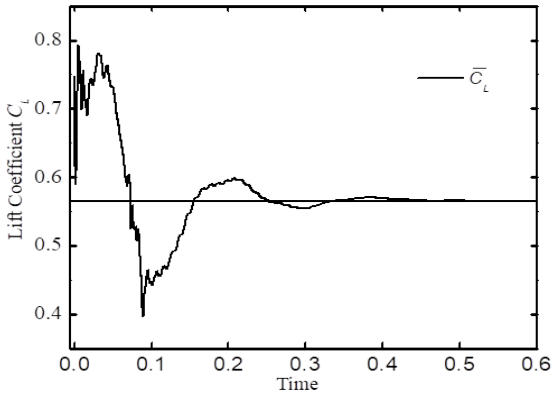

Figure 6(g): Lift coefficient time series for cavitation value 1.1

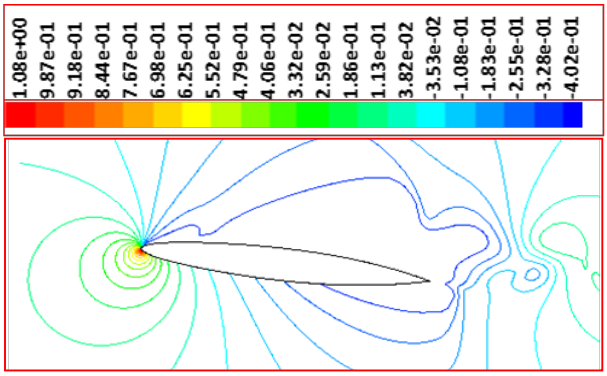

Figure 7(a): Pressure coefficient Contour on foil at cavitation value 0.4

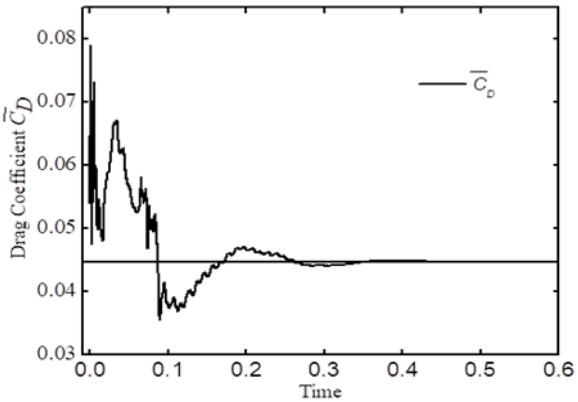

Figure 6(h): Drag coefficient time series for cavitation value 1.1

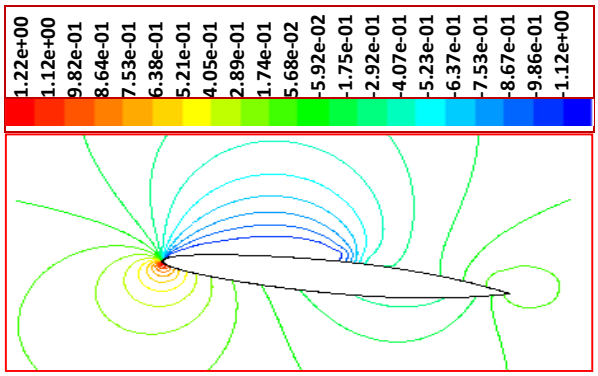

Figure 7(b): Pressure coefficient Contour on foil at cavitation value 0.8

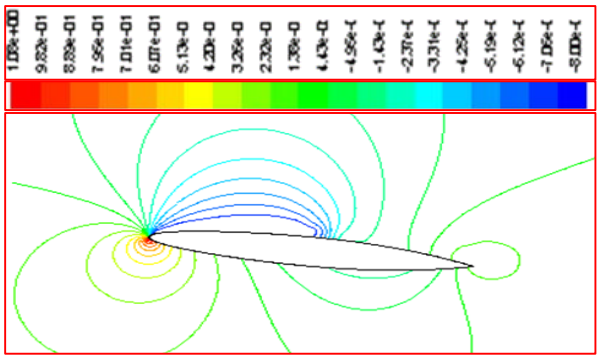

Figure 7(c): Pressure coefficient Contour on foil at cavitation value 0.9

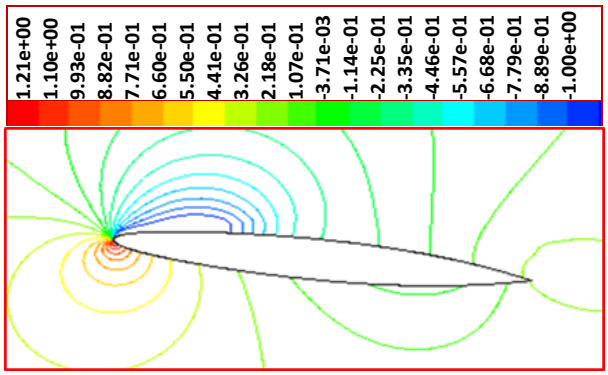

Figure 7(d): Pressure coefficient Contour on foil at cavitation value 1.0

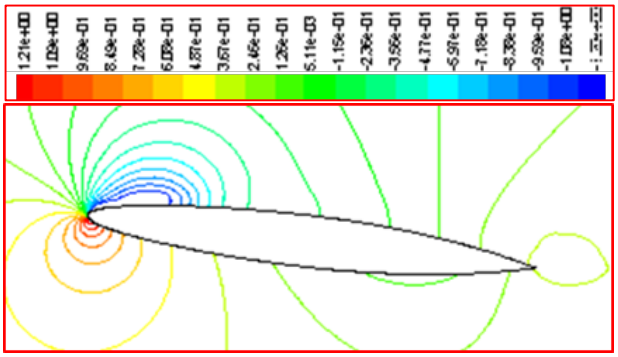

Figure 7(e): Pressure coefficient Contour on foil at cavitation value 1.2

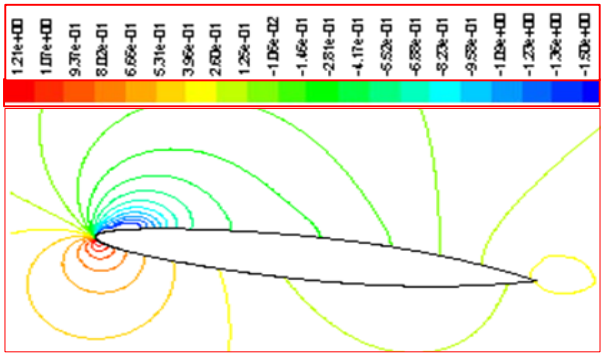

Figure 7(f): Pressure coefficient Contour on foil at cavitation value 1.5

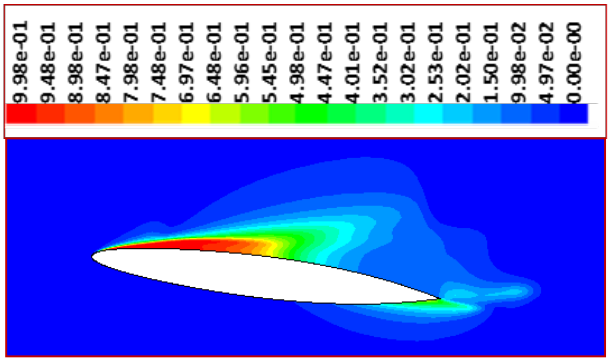

Figure 8(a): Computed vapour volume fraction at cavitation value 0.4

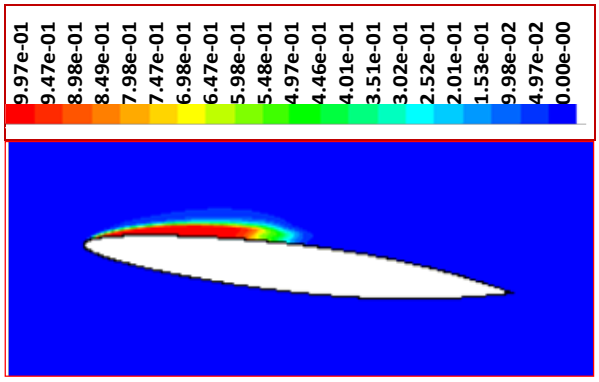

Figure 8(b): Computed vapour volume fraction at cavitation value 0.8

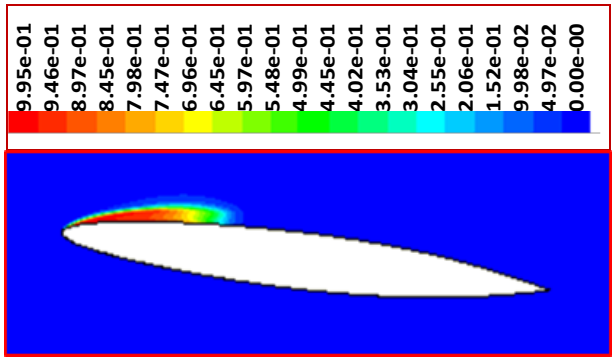

Figure 8(c): Computed vapour volume fraction at cavitation value 0.9

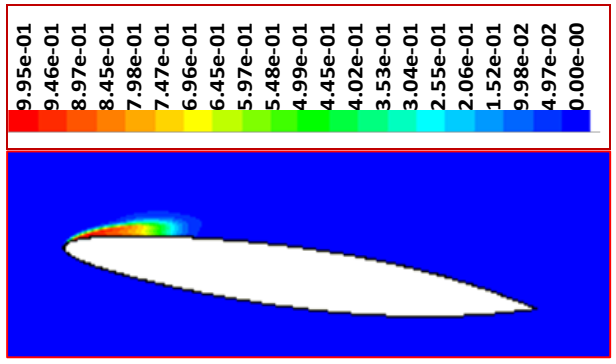

Figure 8(d): Computed vapour volume fraction at cavitation value 1.0

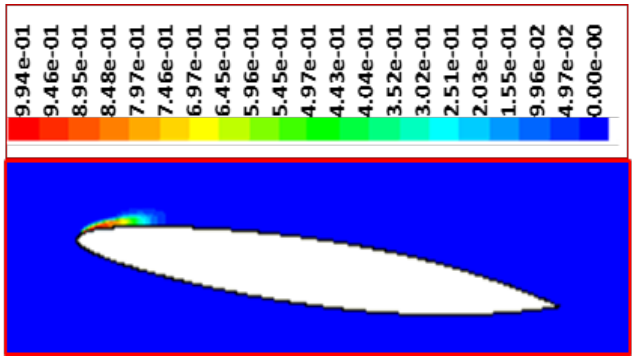

Figure 8(e): Computed vapour volume fraction at cavitation value 1.2

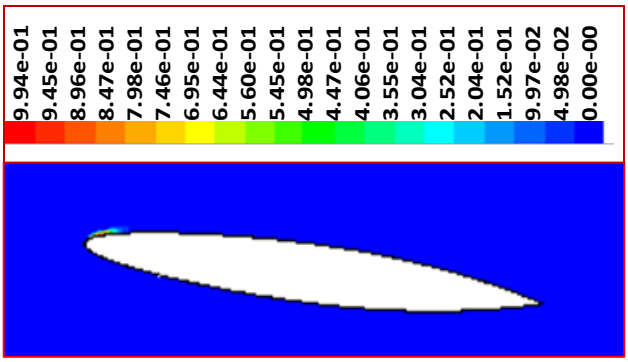

Figure 8(f): Computed vapour volume fraction at cavitation value 1.5

The summary of the time dependent average lift coefficient, drag coefficient, maximum size ($\bar{l}_{max}$) of cavity and maximum width ($\bar{t}_{max}$) of cavity are shown in Table 3 with the various cavitation values respectively. It is seen that the most cavity size and the most cavity width increase with decreasing of cavitation values. A full cavitating flow is developed at σ value 0.4 on the hydrofoil upstream surface.

Table 3
Summary of different cavitation's parameter

Σ	$\bar{l}_{max}$	$\bar{t}_{max}$	$\bar{C}_L$	$\bar{C}_D$
3.5	–	–	0.667	0.0242
1.5	0.098	0.0211	0.582	0.0378
1.2	0.161	0.0329	0.572	0.0425
1.1	0.212	0.0465	0.566	0.0446
1.0	0.251	0.0473	0.560	0.0476
0.9	0.452	0.0772	0.512	0.0783
0.8	0.491	0.0784	0.442	0.0773
0.4	1.001	0.282	0.214	0.0763

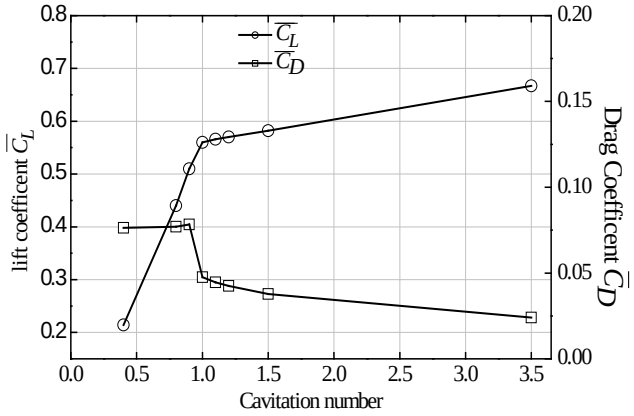

Figure 9: Computed lift and drag coefficient with cavitation values

The computed values of $\bar{C}_L$ and $\bar{C}_D$ together are appeared in Figure 9. It is comprehended that time dependent averaged lift value reduces as decreasing the cavitation number. Moreover, time dependent averaged drag value once almost same at σ value 0.4 to 0.9 and then decline slightly after taking a maximum values at $\sigma = 0.9$ with growing the cavitation number. In addition, it is indicated that the standard deviation become large in a transient range of σ value 0.8 to 1.2.

8. CONCLUTIONS

Finite volume solver associating with implicit RNG k-ε turbulence model and accompanied with two phase flow mixture method is employed to capture irregular cavitating flow all over the CAV2003 hydrofoil. Hydrofoil position angle 7° in flow domain, the maximum values of pressure coefficient in cavitation vicinity increase with the decreasing the σ values, while the cavitation started area retains the unchanged. Cavitation initiation starts at the upstream edge and enlarge along the chord with decreasing the cavitation values. It is observed that at σ value 0.4 the rear surface is entirely covered with fluid vapour and reduce with the increasing the cavitation numbers. Moreover, a transient range of flow is found of σ values from 0.8 to 1.2, where the standard deviation becomes large.

ACKNOWLEDGEMENTS

I would like to expresses my heartfelt thanks and gratitude to MIST authority for giving us the research facilities and all over support throughout this research.

REFERENCES

Brennen C. E. (1995). *Cavitation and bubble dynamics.* Oxford University press, Oxford.

Choudhury D. (1993). *Introduction to the Renormalization Group Method and Turbulence Modeling.* Fluent Inc. Technical Memorandum TM-107.

Dular M., Bacher R., Stoffel B., & Širok B. (2005). Experimental evaluation of numerical simulation of cavitating flow around hydrofoil. *European Journal of Mechanics B/Fluids* 24, 522-538.

Frobenius, M., Schilling, R., Bachert, R., & Stoffel B. (2003, November). Three-dimensional unsteady cavitation effects on a single hydrofoil and in a radial pump – measurements and numerical simulations, Part two: Numerical simulation. Proceedings of the Fifth International Symposium on

Cavitation, Osaka, Japan.

Kawamura T., & Sakuda M. (2003, November). Comparison of bubble and sheet cavitation models for simulation of cavitation flow over a hydrofoil. Fifth International Symposium on Cavitation (Cav2003), Osaka, Japan.

Kothandaraman C. R., & Rudramoorthy R. (2007). *Fluid mechanics and Machinery*. New age international publishers.

Kunz R. F., Boger D. A., Stinebring D. R., Chyczewski T. S., Lindau J. W., Gibeling H. J., Venkateswaran S., Govindan T. R. (2000). *A preconditioned Navier-Stokes method for two-phase flows with application to cavitation prediction*. Computers & Fluids, Vol. 29(8), 850-872.

Karim M., Mostafa N., & Sarker M. M. A. (2010). Numerical study of unsteady flow around a cavitating hydrofoil. *Journal of Naval Architecture and Marine Engineering*, vol. 7, 51-61.

Kubota A., Hiroharu A., & Yamaguchi H. (1992). A new modeling of cavitating flows, a numerical study of unsteady cavitation on a hydrofoil section. *Journal of Fluid Mechanics*, vol, 240, 59–96.

Mortezazadeh M., Katal A., & Javadi K. (2014). Cavitation control on hydrofoil. Proceedings of the International Conference on Heat Transfer and Fluid Flow. Prague, Czech Republic

Mostafa N., Karim M., & Sarker M. M. A. (2016). Numerical Prediction of Unsteady Behavior of Cavitating Flow on Hydrofoils using Bubble Dynamics Cavitation Model. *Journal of Applied fluid Machanic*s, Vol. 9, 1829-1837.

Pouffary B., Fortes-Patela R., & Reboud J. L. (2003, November). Numerical simulation of cavitating flow around a 2D hydrofoil: A barotropic approach. Fifth International Symposium on Cavitation (Cav2003), Osaka, Japan.

Roohi E. & Zahiri A. P. (2012). Numerical simulation of cavitation around a Two-Dimensional Hydrofoil Using VOF Method and LES Turbulence Model. Proceedings of the Eighth International Symposium on Cavitation (CAV 2012). Singapore.

Schnerr G. H. & Sauer J. (2001). Physical and numerical modeling of unsteady cavitation dynamics 4th International Conference on Multiphase Flow, ICMF-2001, New Orleans, USA.

Singhal A. K., Li H., Atahavale M. M., & Jiang Y. (2002). Mathematical basis and validation of the full cavitation model. *Journal of Fluids Engineering*, vol, 124, 617–624.

Stutz B. & Reboud J. L. (2002). Measurements within unsteady cavitation. *Experiments in Fluids*, vol. 29, 545-552.

Yoshinori S., Ichiro N., & Tosshiaki I. (2003). Numerical analysis of unsteady vaporous cavitating flow around a hydrofoil. Fifth International Symposium on Cavitation (Cav2003), Osaka, Japan.